In situ control of dewetting of Cu thin films in graphene chemical vapor deposition

In situ control of dewetting of Cu thin films in graphene chemical vapor deposition

L. Croin[1,2], E. Vittone[3] and G. Amato[1]

[1] The Quantum Research Laboratory, INRIM, strada delle Cacce 91, I-10135, Torino, Italy

[2] Dept. of Applied Science and Technology - DISAT, Politecnico di Torino, Corso Duca degli Abruzzi 24, I-10129, Torino, Italy

[3] Physics Dept. and NIS Interdepartmental Centre, University of Turin, Via Pietro Giuria 1, I-10125, Torino, Italy.

E-mail: l.croin@inrim.it

Abstract.

Chemical Vapor Deposition (CVD) on Cu thin films is a promising approach for the large area formation of graphene on dielectric substrates, but a fine control of the deposition parameters is required to avoid dewetting of the Cu catalyst. In this paper we report on the study of the Cu dewetting phenomena by monitoring the intensity of the infra-red emission from the film surface during Rapid Thermal CVD of graphene. The reduction of Cu film coverage consequent to dewetting is detected as a variation of sample's emissivity. Results indicate three time constants of dewetting, describing three typical stages, hole formation, propagation and ligament breakup. Slowing the first incubation stage by tuning pressure in the chamber allows for an effective surface activation resulting in the deposition of graphene at temperatures lower than in the case of Cu foils.

Keywords:

dewetting, CVD graphene synthesis, structural transformation, chemical vapor deposition, infra-red emission, electron microscopy.

1. Introduction

Compared to the wealth of information available in current literature about the CVD (Chemical Vapor Deposition) of graphene onto Cu foils [1], there is a dearth of experimental studies dealing with the use of Cu thin (< 500 nm) films as substrates [2-5]. However, these latter offer several advantages: first, they are deposited in High Vacuum environments and show less contamination than commercial foils, second, the small amount of the Cu substrate make the graphene transfer process much less invasive, third, the use of films makes the process more compatible with the current microelectronics technology.

One of the most critical factors which hinder the adoption of Cu thin films as substrates for CVD deposition of graphene is their metastability of the films, since undergo agglomeration (more commonly defined as dewetting) if treated at high temperatures. Such effect is well known from several decades [6], and theoretically studied since the 1970's. Dewetting is known to appear in films with different crystallographic quality, no matter if mono-crystalline [7] or poly-crystalline [8]. In the latter case, a simple model based onto balance of the surface tension [8] at a grain boundary can be drawn. The equilibrium between the grain boundary (GB) energy γ_{GB} and the surface energy γ_s allows defining the angle φ, which determines the curvature of the grain surface as [9]:

$$\varphi = \sin^{-1}\left(\frac{\gamma_{GB}}{2\cdot\gamma_s}\right), \tag{1}$$

and calculations lead to obtain the depth δ of the forming groove at the GB as:

$$\delta = \frac{R\cdot(2-3\cdot cos\varphi+cos^3\varphi)}{3\cdot sin^3\varphi} \tag{2}$$

where R is the average radius of the grain. When δ equals the film thickness h_0, a hole is formed in the film. The stage prior to hole opening is defined as incubation stage.

When using thin films of metal catalyst (e.g. Cu) for graphene CVD, researchers tend to increase the hole incubation time (t_0), generally by using thick films [10-15] (≥500 nm). As a matter of fact, thicker Cu films can be simply treated as foils, then applying the same deposition conditions, with comparable results [10]. Nevertheless, deep grooves at GBs are likely formed and the graphene sheet may pucker in some regions when transferred, as elucidated by the AFM (Atomic Force Microscope) image in figure 1. Such puckering has not to be confused with wrinkles due to difference of thermal expansion between graphene and the substrate [8], because it is observed onto the transfer destination substrate, solely [16].

However, film dewetting should not merely be considered as an obstacle, but as an additional resource to open alternative chances for the large scale graphene synthesis. For example, the possibility to carefully lay down the graphene sheet onto the substrate underlying the Cu film (typically SiO_2), just during deposition, avoids cumbersome and time consuming transfer processes [4]. In addition, in a film subjected to dewetting, the surface is close to being liquid. This is considered as necessary for optimal graphene growth on Cu [1].

Here, we report a study of the substrate dewetting and propose an approach to improve the controllability and reproducibility of the CVD deposition process of graphene on thin (< 500 nm) Cu films.

2. Experimental

Cu films of 200 nm and 350 nm, evaporated at a rate of 0.17 nm/s onto oxidized Si substrates at pressures in the 10^{-5} Pa range have been employed for the purpose. Substrates have been cleaned in a class 100 clean room by sonication in acetone and isopropanol, then rinsed in deionized water, dried in N_2 flow and rapidly loaded into the evaporator chamber. Just after Cu evaporation the specimen has been transferred into a Jipelec JetFirst 100 Rapid Thermal

CVD (RTCVD) system, and promptly evacuated down to the 10^{-3} Pa range to minimize oxidation due to air exposure. The RTCVD apparatus allows heating and cooling at high rates (tens °C/s), making the interpretation of dewetting dynamics simpler that in a conventional resistively heated furnace. In the RTCVD system, a wafer is placed horizontally onto three quartz pins and heated by means of an array of halogen lamps on the top of the chamber.

For the aim of this work, the sample is mounted upside down in the chamber (see figure 2) and its temperature is measured by three thermocouples in contact with the sample back face.

A quartz window allowed thermal radiation emission from the Cu layer to be monitored by means of a pyrometer with a centred wavelength of λ=5.14 μm (figure 2).

Being the signal of the pyrometer proportional to the Planck's black body radiation law and to the body emissivity (ε) and since the emissivity of the film (ε_{Cu}) is approximately 2 times lower that the emissivity of the substrate (ε_{SiO_2}), we expect to monitor the dewetting process as a gradual transition from ε_{Cu} to ε_{SiO_2}:

$$\varepsilon_{eff}(t) = \varepsilon_{Cu} \cdot x(t) + \varepsilon_{SiO_2}[1 - x(t)] \rightarrow B(t) = B_{Cu} \cdot x(t) + B_{SiO_2}[1 - x(t)], \qquad (3)$$

Where ε_{eff} is the effective emissivity of partially covered SiO_2 surface (film experiencing dewetting) and $x(t)$ is the percentage of the surface covered with Cu, which decreases with time; correspondingly, on the right side, $B(t)$ is the relevant signal of the pyrometer at time t and B_{SiO_2}, B_{Cu} are the signals measured from pure SiO_2 and Cu samples, respectively.

We measured the final relative Cu coverage x_{SEM} by analysing the SEM (Scanning Electron Microscope) micrographs of the dewetted samples using the ImageJ software [17]. Markers on the right side of figure 3 represent the B values calculated by eq. (3) for the Cu coverage given by SEM analysis. The excellent agreement with the asymptotic values of B(t) detected by the pyrometer validates the model and supports the assumption that the surface roughness radiation scattering plays a negligible role in the dewetting monitoring.

3. Results and discussion

Focusing on the response shown in figure 3 for, e.g., T= 600 °C in vacuum, after a first signal rise due to sample heating, we clearly observe the incubation time of dewetting as a constant signal value for a time interval t_0, where a complete Cu surface coverage persists, i.e. $x(t \leq t_0)$= 1 and $\varepsilon_{eff}=\varepsilon_{Cu}$. Then, holes open, Cu retracts, and ε_{eff} increases to approach ε_{SiO_2}. It is worth noting that for higher T, the incubation time falls down dramatically: as shown in the inset (a) of figure 3, the Cu film surface just after the heating ramp (20 °C·s^{-1} rate) up to 700 °C already shows the presence of grains with bumped surface. According to the above discussion, in the neighbouring GBs, holes are likely to form. In other words, if T is high enough, the incubation stage of dewetting already starts during heating.

The inset (b) of figure 3 displays the complementary curve of the dewetting-related rise at 800 °C in a semi-log plot, and indicates a clear double exponential behaviour, i.e.:

$$B(\infty) - B(t) = B_1 \cdot e^{-\frac{t}{t_1}} + B_2 \cdot e^{-\frac{t}{t_2}} \quad (4)$$

Accordingly, three different peculiar time constants, relevant to three distinct stages, can be extracted from the monitoring of the dewetting phenomenon: the incubation time t_0 in the constant portion of the B(t) curve and the fast (t_1) and slow (t_2) exponential components.

No previous theoretical models of dewetting consider such a double exponential time evolution, however, there is general consensus about three different stages in dewetting: hole formation, hole growth and impingement, and ligament breakup [7,18].

Figure 4(a) compares the time constant t_0 values extracted at the chosen temperatures for the 200 nm and 350 nm thick films, both at a pressure of P=0.1 Pa. As expected, the characteristic time t_0 increases with thickness, and dramatically decreases with T in both sets of samples. A similar thickness and T-dependence of t_1 and t_2 is observed, as elucidated by figure 4(b), which summarizes the results for t_1. However, it is worth noticing that the slow

portion of the dewetting process, described by time constant t_2, maintains a nearly constant value of about 100 s, regardless the thin film thickness and the process temperature.

The micrograph in the inset of figure 4(b) shows the morphology of a Cu film extracted from the chamber after $t=t_0+t_1$ and confirms that t_1 is related to the hole growth stage of dewetting.

As a preliminary conclusion, we can then affirm that the dynamic surface, close to being a liquid [1], as requested for optimal graphene growth on Cu, is attainable in films at temperatures lower than in the case of foils (T> 1000 °C).

Such high T values seem necessary, even in cases where C precursors catalysing at lower T are employed [19]. At such T values, moreover, consistent Cu sublimation occurs, the Cu vapour pressure reaching 10^{-2} Pa [1]. Even if the role of sublimation is still unclear, it has been demonstrated that in foils it leads to Cu step retraction [20]. Such sublimation is slowed in regions covered by graphene, causing Cu steps to be trapped under graphene, thereby creating mounds and roughening the surface topography. Actually, the low temperatures required to activate the Cu thin films inhibit sublimation and can presumably contribute to mitigate this effect [21]. In fact, the analysis of Cu films dewetting test corroborate the hypothesis of a minor role played by sublimation during the thermal process for temperatures lower than 900 °C. The analysis was carried out by taking into account the final relative coverage x_{SEM} of h_0=200 nm Cu thin film after thermal annealing at different temperatures. The height of Cu particles ($h= h_0/x_{SEM}$), calculated under the assumption that volume is conserved, was then compared with the average height $<h>$ of particles extracted from SEM micrographs (see Fig. 5(b)) of the Cu surface. Figure 5(a) shows a comparison between the two sets of data: only the 900 °C process shows a discrepancy suggesting that the Cu volume is not conserved, i.e. a minor sublimation occurs.

Dewetting dynamics depend on both temperature and film thickness but a further dependence on pressure in chamber and gas composition is expected. In principle, this allows to increase the number of degrees of freedom for controlling the system.

Several authors employ H_2 to reduce the Cu oxide layer and activate the catalyst surface prior to graphene deposition [10,15]. There is no general consensus, however, on the beneficial [22] or detrimental [11] effect of H_2 addition to carbon-based precursors during the deposition step. To ascertain the role of H_2 on the dewetting process, solely, we carried out the preliminary studies by exposing the film to H_2 for its total duration. Results are summarized in figure 4, which shows that the dewetting behaviour of the thinner films (200 nm) approaches that of thicker ones (350 nm) when H_2 is fluxed in the chamber at a pressure of 25 Pa, although we observe a steeper drop of t_0 with T. According to eqs. (1), (2), this can be related to the noticeable reduction of γ_s at the grain surface due to interaction with H atoms.

This conclusion is supported by the observation of the Cu surface just after the heating step: figure 6 compares the SEM tilted views of Cu films heated up to 700 °C in vacuum and at 25 Pa, H_2 atmosphere, respectively. The reduction of grains with bumped surfaces is noticeable.

To check if this effect is somehow related to chemical reduction of Cu by H_2, or to formation of hydrides onto its surface, as suggested by A. Geissler et al. [23] who observed effects of higher H_2 pressures onto dewetting dynamics, we reproduced the process with an inert gas like Ar at 25 Pa. In this case, the incubation time t_0 further increases up to t_0>1500 s in a 200 nm thick Cu film at 800 °C, suggesting a physical, rather than chemical, interaction of the gas with the film surface. Interestingly, the pyrometer signal increases as soon as the Ar flow stops, even if with a slower dynamics than in the vacuum case. Such effect is shown in figure 7 (a), which compares the pyrometer signal variation in different working conditions. The slower ascent of the pyrometer signal in the latter case suggests that few holes are opened

during heating in Ar atmosphere. According to the model previously described, if hole incubation is inhibited by the presence of gas molecules at the grain surface, the average groove depth $<\delta>$ is expected to be smaller with respect to the vacuum case. Then, when gas is pumped away, fewer holes appear and the fraction of uncovered SiO_2 grows slower than in the case of incubation in vacuum (figure 7 (a)). In other words, the time constant t_1, governing the hole opening stage, depends on the previous hole incubation process in our detection system.

These results confirm the commonly accepted *scenario* in which the growth of graphene on Cu films presents limitations with respect to Cu foil substrates: to get rid of film dewetting one requires: a) relatively thick films (> 500 nm), b) moderate temperatures (< 1000 ° C), c) high pressures (close to atmospheric). These, at first sight, limitations, can be exploited, in our opinion, through a careful *in situ* control of film dewetting. Then, the careful dosage of the gas composition and pressure introduces additional degrees of freedom to optimize the reactivity of the Cu surface before introducing the reactive species.

Graphene pre-deposition treatments of the substrate normally employ both H_2 and Ar, the first to reduce Cu oxide [24,25] and the second to more efficiently preserve the Cu film from dewetting. With the aim of studying the possibility of activating the Cu surface, preserving the dewetting at the same time, we prepared two recipes, a *soft* one, in which H_2 is fluxed in the chamber for 5 min, followed by Ar for 1 min, and a *hard* one in which a Ar/H_2 mixture (10:1 flux ratio) is fluxed for 6 min. Pressure was kept at 25 Pa in both cases. The Cu substrate was 200 nm thick. Instead of the more commonly used methane, which is catalysed at T values outside our range of interest, we used ethanol [19,26,27] at T values in the range of 650 °C to 800 °C. It is worth noting that, when ethanol vapors are fluxed, no emissivity-related rise in the pyrometer response is detected in the deposition time window, i.e. dewetting does not occur during deposition for times up to 1500 s. After closing the ethanol

source, Ar is fluxed again in the chamber during the cooling stage to preserve the Cu film underneath.

It is worthy to note, that either the pre-deposition or the graphene deposition processes are not optimized. As previously discussed, the aim of this work is to identify the possibility of controlling dewetting in the catalyzing film, in order to obtain a dynamic surface, required for graphene deposition, avoiding the film rupture at the same time. To achieve optimal results, several parameters have to be finely adjusted, namely, film thickness, temperature, pressure chamber, and gas composition and fluxes in both pre-deposition and deposition steps. As an example, no H_2 is added to carbon source during deposition, as it has been proved that small amounts of H_2 can be beneficial to the graphene's quality [19]. In both the recipes, a Cu foil has been added in the deposition chamber as a control, to evidence the different surface behaviour of the two systems.

Raman spectroscopic analysis of graphene obtained in this way indicates that on the cm^2 scale a uniform double layer has been obtained, as suggested by the intensity ratio of 2D and G peaks (figure 8). Nevertheless, the intensity of the D peak at 1380 cm^{-1} changes with the chosen recipe, being higher in the *soft* process. As previously mentioned, the quality of graphene film is not optimal, but a clear trend is observed. The effect of the different pre-deposition recipes requires deep investigations that are underway, but it seems clear that in the *soft* case, a larger number of nucleation sites for graphene gives rise to smaller domains, i.e. to nanocrystalline graphene [28]. A more strict control of dewetting with the aid of Ar, on the contrary (*hard* recipe) seems to reduce such nucleation site density, giving rise to larger domains. Interestingly, the pyrometer signal (figure 7 (b)) keeps constant during deposition only in the *hard* case, confirming the key role played by the pre-deposition on the deposition step. This envisages the possibility of correlating the final graphene quality with the time evolution of the signal from the substrate. Last, it is important to note that the same

deposition conditions yield a higher quality graphene on Cu films rather than on foils. In this case, in fact, the Raman spectrum is indicative for a nanocrystalline multilayered graphene film [29]. Similar, unsatisfactory quality has been obtained on the Cu foil using different pre-deposition recipes, including pure H_2 fluxing or high vacuum annealing, but leaving out any temperature activation (around 1000 °C) [26] of the surface. This confirms that, in the investigated T range, surface mobility of Cu atoms increases more in films than in foils, as a consequence of the different balance between the surface and the GB energies, as evidenced in equations (1) and (2).

4. Conclusions

In conclusion, we have shown that in a standard RTCVD system, the dewetting of the catalyst film can be easily monitored *in situ* by optically recording its infra-red emission. Incubation of dewetting in vacuum is dramatically short in the case of thinner Cu films and, for T> 700 °C, i.e. it occurs already during the heating stage. Addition of H_2 in this stage slows-down hole incubation as well as reduces Cu oxide. Dewetting can be further slowed by using Ar or Ar/H_2 mixtures. Tuning the pressure in the chamber is an easy way to control Cu mobility and to preserve the film surface, in order to reach the optimal conditions for graphene growth. In other words, graphene is grown during a prolonged dewetting incubation time. Differently from foils, in which the graphene quality is highly dependent on the temperature (around 1000 °C), no matter if in the pre-deposition [26] or deposition [19] step, our results demonstrate that Cu films can be efficiently activated at lower T values and the process can be fully controlled by adjusting several parameters (besides the film thickness and T) like the pressure in chamber, the gas composition, and the pre-deposition duration.

Acknowledgments

Authors are indebted with G. Milano for setting up the dewetting measurement system and with Dr. A. Damin (NIS Centre of Excellence, University of Turin) for Raman spectroscopic investigations. SEM analysis has been performed at Nanofacility Piemonte, a laboratory funded by Compagnia di San Paolo, which also partially supported this work within the University of Torino-Compagnia di San Paolo-projects ORTO11RRT5, 2011- Linea 1A and call “Call1-D15E13000130003”.

References

[1] N. C. Bartelt, K.F. McCarty, Graphene growth in metal substrates, MRS Bulletin 37 (2012) 1158-1165, and references therein.

[2] Y.-H. Lee and J.-H. Lee, Scalable growth of free-standing graphene wafers with copper(Cu) catalyst on SiO2/Si substrate: Thermal conductivity of the wafers, Appl. Phys. Lett. 96 (2010) 083101.

[3] C.-Y. Su, A.-Y. Lu, C.-Y. Wu, Y.-T. Li, K.-K. Liu, W. Zhang, S.-Y. Lin, Z.-Y. Juang, Y.-L. Zhong, F.-R. Chen, L.-J. Li, Direct Formation of Wafer Scale Graphene Thin Layers on Insulating Substrates by Chemical Vapor Deposition, Nano Lett. 11 (2011) 3612-3616.

[4] A. Ismach, C. Druzgalski, S. Penwell, A. Schwartzberg, M. Zheng, A. Javey, J. Bokor, Y. Zhang, Direct Chemical Vapor Deposition of Graphene on Dielectric Surfaces, Nano Lett. 10 (2010) 1542-1548.

[5] T. Kaplas, D. Sharma, Y. Svirko, Few-layer graphene synthesis on a dielectric substrate, Carbon 50 (2012) 1503-1509.

[6] A. E. B. Presland, G. L. Price, D. L. Trimm, Hilock formation by surface diffusion on thin silver films, Surf. Sci. 29 (1972) 424-434.

[7] J. Ye, C. V. Thompson, Mechanisms of complex morphological evolution during solid-state dewetting of single-crystal nickel thin films, Appl. Phys. Lett. 97 (2010) 071904; J. Ye, C. V. Thompson, Anisotropic edge retraction and hole growth during solid-state dewetting of single crystal nickel thin films, Acta Mater. 59 (2011) 582-589.

[8] D. J. Srolovitz and S. A. Safran, Capillary instabilities in thin films. I. Energetics, J. of Appl. Phys. 60 (1986) 247-254.

[9] C. V. Thompson, Solid-state dewetting of thin films, Ann. Rev. of Mat. Res. 42 (2012) 399-434.

[10] M. P. Levendorf, C. S. Ruiz-Vargas, S. Garg, J. Park, Transfer-free batch fabrication of single layer graphene transistors , Nano Lett. 9 (2009) 4479-4483.

[11] L. Tao, J. Lee, H. Chou, M. Holt, R. S. Ruoff, D. Akinwande, Synthesis of High Quality Monolayer Graphene at Reduced Temperature on Hydrogen-Enriched Evaporated Copper (111) Films, ACS Nano 6 (2012) 2319-2325; L. Tao, J. Lee, M. Holt, H. Chou, S. J. McDonnell, D. A. Ferrer, M. G. Babenco, R. M. Wallace, S. K. Banerjee, R. S. Ruoff, D. Akinwande, Uniform Wafer-Scale Chemical Vapor Deposition of Graphene on Evaporated Cu (111) Film with Quality Comparable to Exfoliated Monolayer, J. Phys. Chem. C 116 (2012) 24068-24074.

[12] Y. Lee, S. Bae, H. Jang, S. Jang, S.-E. Zhu, S. H. Sim, Y. I. Song, B. H. Hong, J.-H. Ahn, Wafer-Scale Synthesis and Transfer of Graphene Films, Nano Lett. vol. 10 no. 2 (2010) 490–493.

[13] B. Hu, H. Ago, Y. Ito, K. Kawahara, M. Tsuji, E. Magome, K. Sumitani, N. Mizuta, K. Ikeda, and S. Mizuno, Epitaxial growth of large-area single-layer graphene over Cu(111)/sapphire by atmospheric pressure CVD, Carbon 50 (2012) 57-65.

[14] M. Piazzi, L. Croin, E. Vittone, G. Amato, Laser-induced etching of few-layer graphene synthesized by Rapid-Chemical Vapour Deposition on Cu thin films, SpringerPlus 1 (2012) 52.

[15] C. Mattevi, H. Kim, and M. Chhowalla, A review of chemical vapour deposition of graphene on copper, J. Mater. Chem. 21 (2011) 3324-3334.

[16] G. Amato, E. Simonetto, L. Croin, E. Vittone, A New Transfer Technique for Graphene Deposited by CVD on Metal Thin Films, MRS Proceedings 1658 (2014) mrsf13-1658-rr15-95 doi:10.1557/opl.2014.506.

[17] ImageJ public domain software available at URL: http://imagej.nih.gov/ij/ .

[18] R. Saxena, M. J. Frederick, G. Ramanath, W. N. Gill, J. L. Plawsky, Kinetics of voiding and agglomeration of copper nanolayers on silica, Phys. Rev. B 72 (2005) 115425.

[19] G. Faggio, A. Capasso, G. Messina, S. Santangelo, Th. Dikonimos, S. Gagliardi, R. Giorgi, V. Morandi, L. Ortolani, N. Lisi, High-Temperature Growth of Graphene Films on Copper Foils by Ethanol Chemical Vapor Deposition, J. Phys. Chem. C 117 (2013) 21569-21576.

[20] J.M. Wofford, S. Nie, K.F. McCarty, N.C. Bartelt, O.D. Dubon, Graphene Islands on Cu Foils: The Interplay between Shape, Orientation, and Defects, Nano Lett. 10 (2010) 4890-4896.

[21] J. Perdereau, G. E. Rhead, Leed studies of adsorption on vicinal copper surfaces, Surf. Science 24 (1971) 555-571.

[22] I. Vlassiouk, M. Regmi, P. Fulvio, S. Dai, P. Datskos, G. Eres, S. Smirnov, Role of Hydrogen in Chemical Vapor Deposition Growth of Large Single-Crystal Graphene, ACS Nano 5 (2011) 6069-6076.

[23] A. Geissler, M. He, J.-M. Benoit, P. Petit, Effect of Hydrogen Pressure on the Size of Nickel Nanoparticles Formed during Dewetting and Reduction of Thin Nickel Films, J. Phys. Chem. C 114 (2010) 89-92.

[24] J. S. Lewis, The reduction of copper oxide by hydrogen, J. Chem. Soc. 0 (1932) 820–826.

[25] R. N. Pease, H. S. Taylor, The reduction of copper oxide by hydrogen, J. Am. Chem. Soc. 43 (1921) 2179-2188.

[26] P. Zhao, A. Kumamoto, S. Kim, X. Chen, B. Hou, S. Chiashi, E. Einarsson, Y. Ikuhara, and S. Maruyama, Self-Limiting Chemical Vapor Deposition Growth of Monolayer Graphene from Ethanol, J. Phys. Chem. C 117 (2013) 10755-10763.

[27] S. Duan and S. Senkan, Catalytic Conversion of Ethanol to Hydrogen Using Combinatorial Methods, Ind. Eng. Chem. Res. 44 (2005) 6381-6386.

[28] S. J. Chae, F. Guenes, K. K. Kim, E. S. Kim, G. H. Han, S. M. Kim, H.-J. Shin, S.-M. Yoon, J.-Y. Choi, M. H. Park, C. W. Yang, D. Pribat, Y. H. Lee , Synthesis of Large‐Area Graphene Layers on Poly‐Nickel Substrate by Chemical Vapor Deposition: Wrinkle Formation, Adv. Mater. 21 (2009) 2328-2333.

[29] A. Turchanin, D. Weber, M. Büenfeld, C. Kisielowski, M.V. Fistul, K.B. Efetov, T. Weimann, R. Stosch, J. Mayer, A. Gölzhäuser, Conversion of Self-Assembled Monolayers into Nanocrystalline Graphene: Structure and Electric Transport, ACS Nano 5 (2011) 3896-3904.

Figure captions

Figure 1. AFM image of a graphene sheet transferred onto PMMA. Due to its viscosity, PMMA does not fill the deep grooves when spun onto the film. Graphene, which follows the Cu film corrugations, is puckered in those regions after transfer (circled areas).

Figure 2. Scheme of the RTCVD system.

Figure 3. A collection of pyrometer responses B(t) taken on a 200 nm thick Cu film dewetted in vacuum at different temperatures. B(∞) is the response value at saturation. Initial rise corresponds to the heating ramp, whereas the second one is related to the change in emissivity due to hole opening and coalescence in the Cu film. The incubation stage is clearly visible in between the two rises for the curves at lower temperatures. Arrows on the right indicate B values, as evaluated by inserting in eq. (3) the final surface coverage by software analysis on SEM micrographs. Inset (a): surface topography of a Cu film extracted just after heating up to 700 °C, showing the presence of surface bumps. Inset (b): the complementary curve of the emissivity-related rise at 900 °C displayed in the main graph: a satisfactory fit (full line) is obtained by using a double exponential function (dashed lines).

Figure 4. A summary of characteristic times of dewetting in Cu films. Closed symbols refer to the 200 nm thick film, whereas open ones pertain to the 350 nm one. (a) t_0 vs. T: red squares and blue triangles are relevant to annealing in vacuum and H_2 respectively. Data at 900 °C are missing because hole opening already occurs during heating and t_0 cannot be

evaluated. (b), t_1 vs. T. At 600 °C (350 nm and 200 nm in H_2), the pyrometer signal was almost constant in the investigated time interval: t_0 is then assumed to be longer than 10^3 s (arrow in figure 4a) and t_1 is missed. Inset: surface topography of a 350 nm film extracted from the chamber after $t = t_0 + t_1$ at 700 °C.

Figure 5. (a) Comparison of the measured height $\langle h \rangle$ with the height h of dewetted particles calculated if Cu volume were conserved. The error bar is related to dispersion of the particle heights. No sublimation occurs between 600 and 800 °C, while for 900 °C process a discrepancy is observed. (b) SEM micrograph of a section of a sample after a 800 °C thermal process.

Figure 6. Tilted SEM images of Cu films, 200 nm thick, heated up to 700 °C in vacuum (top) and H_2 atmosphere (bottom), promptly cooled and extracted out of the chamber. The percentage of bumped grains is reduced in presence of H_2.

Figure 7. (a) A collection of dewetting curves obtained at different conditions and T= 800 °C. The arrow indicates the interruption of Ar flux in the chamber in the Ar+Vacuum process. In the case of gas flow (green and cyan curves), the pressure was kept at 25 Pa. (b) Evolution of the pyrometer signals during the *hard* and *soft* recipes (T=700 °C).

Figure 8. Typical Raman spectra of graphene deposited on Cu by means of the processes described in the text at T=700 °C. From top to bottom: *hard* recipe (red), *soft* recipe (blue), and foil (with *hard* recipe in this case, but results do not depend on the pre-treatment). To avoid background luminescence from Cu, illumination at 442 nm has been employed [14].

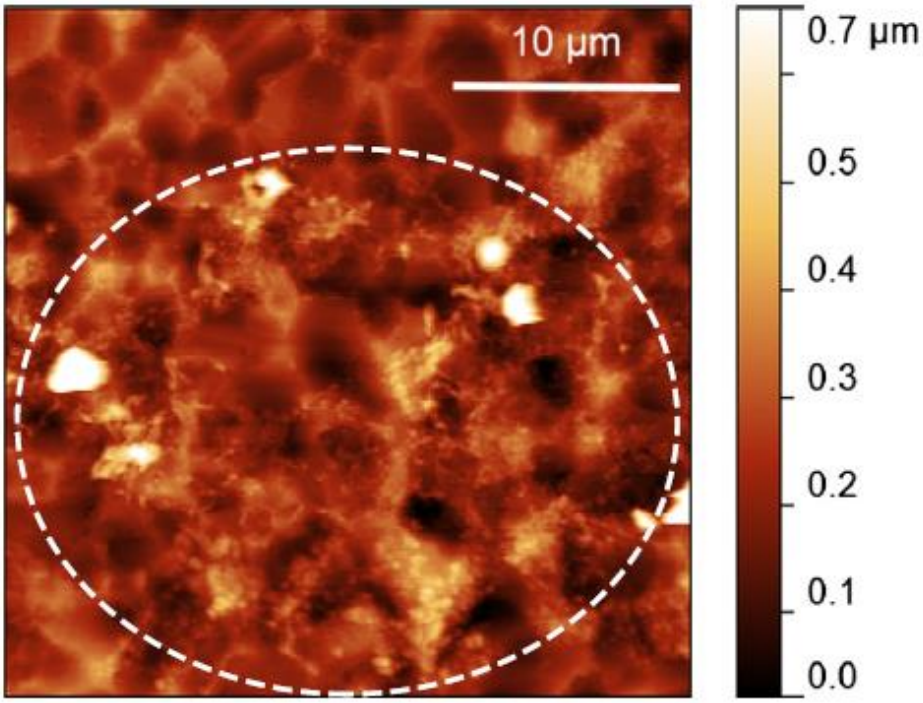

Fig. 1. AFM image of a graphene sheet transferred onto PMMA. Due to its viscosity, PMMA does not fill the deep grooves when spun onto the film. Graphene, which follows the Cu film corrugations, is puckered in those regions after transfer (circled areas).

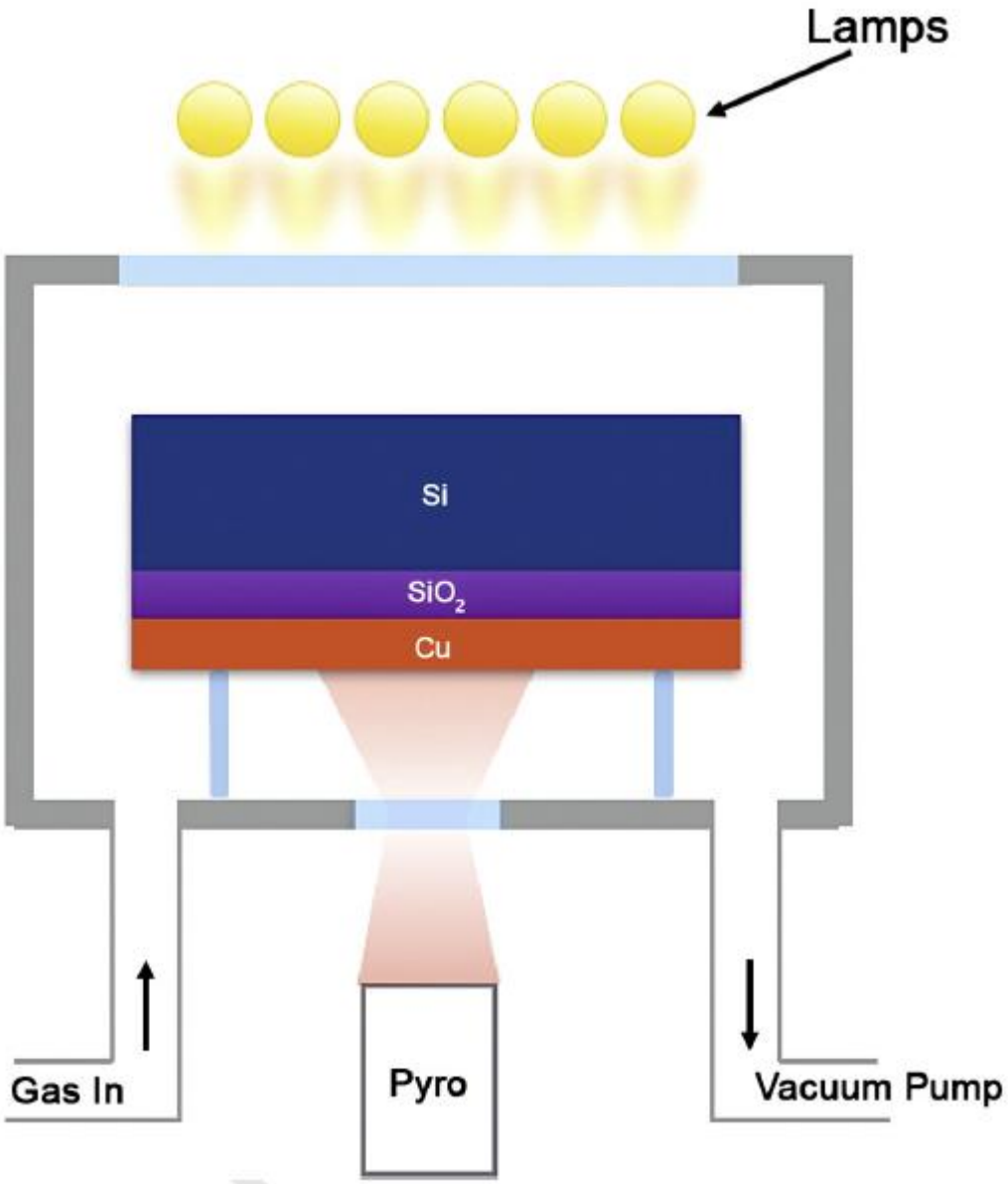

Fig. 2. Scheme of the RTCVD system.

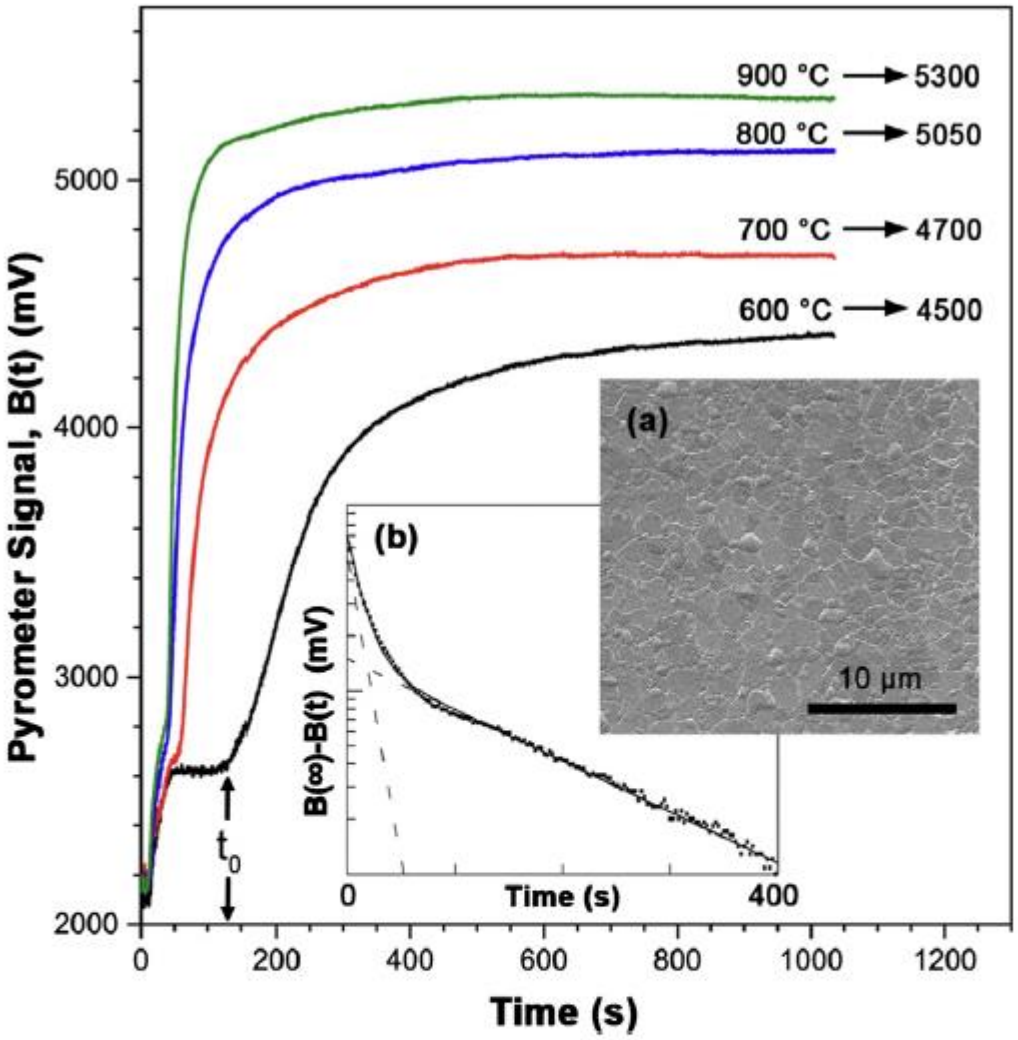

Fig. 3. A collection of pyrometer responses B(t) taken on a 200 nm thick Cu film dewetted in vacuum at different temperatures. B(∞) is the response value at saturation. Initial rise corresponds to the heating ramp, whereas the second one is related to the change in emissivity due to hole opening and coalescence in the Cu film. The incubation stage is clearly visible in between the two rises for the curves at lower temperatures. Arrows on the right indicate B values, as evaluated by inserting in Eq. (3) the final surface coverage by software analysis on SEM micrographs. Inset (a): surface topography of a Cu film extracted just after heating up to 700 °C, showing the presence of surface bumps. Inset (b): the complementary curve of the emissivity-related rise at 900 °C displayed in the main graph: a satisfactory fit (full line) is obtained by using a double exponential function (dashed lines).

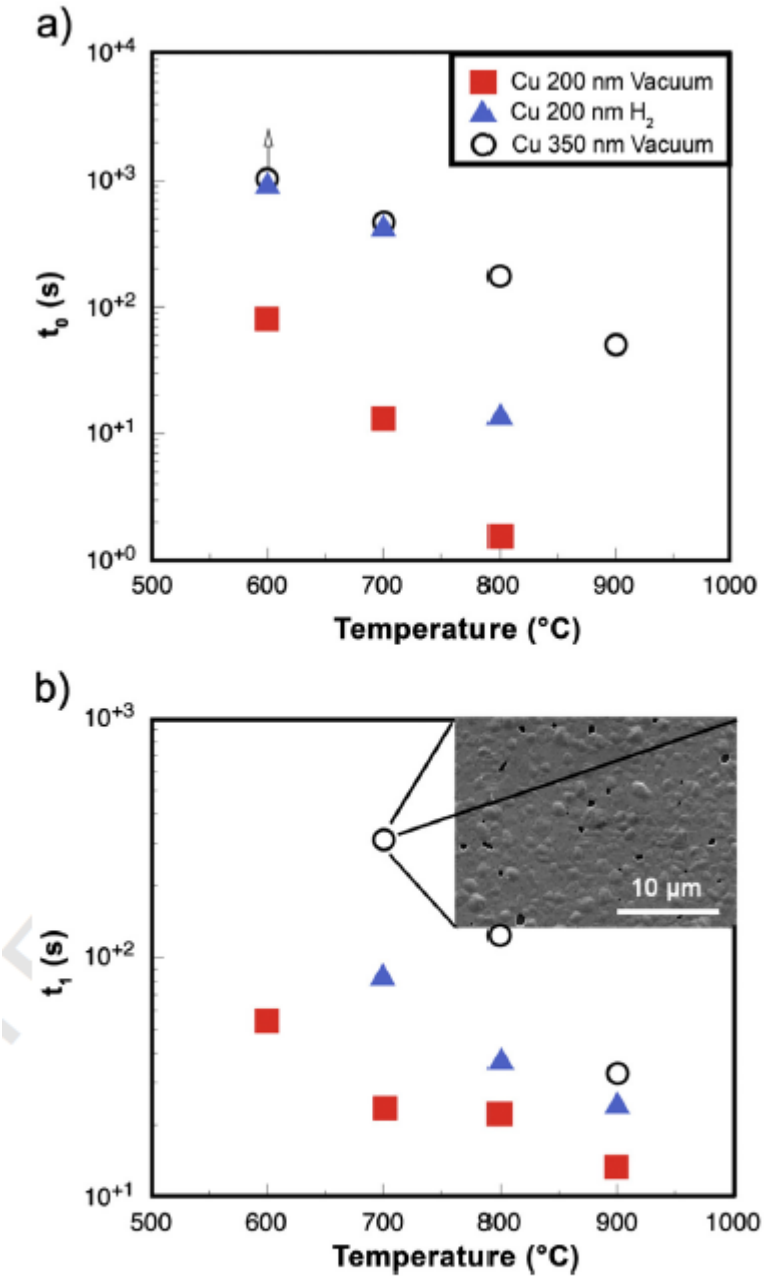

Fig. 4. A summary of characteristic times of dewetting in Cu films. Closed symbols refer to the 200 nm thick film, whereas open ones pertain to the 350 nm one. (a) t_0 vs. T: red squares and blue triangles are relevant to annealing in vacuum and H_2 respectively. Data at 900 °C are missing because hole opening already occurs during heating and t_0 cannot be evaluated. (b) t_1 vs. T at 600 °C (350 nm and 200 nm in H_2), the pyrometer signal was almost constant in the investigated time interval: t_0 is then assumed to be longer than 10^3 s (arrow in (a)) and t_1 is missed. Inset: surface topography of a 350 nm film extracted from the chamber after $t = t_0 + t_1$ at 700 °C. (For interpretation of the references to color in this figure legend, the reader is referred to the web version of this article.)

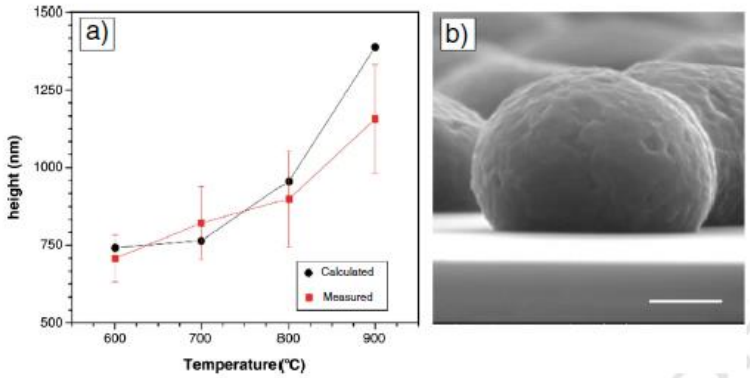

Fig. 5. (a) Comparison of the measured height <*h*> with the height *h* of dewetted particles calculated if Cu volume was conserved. The error bar is related to dispersion of the particle heights. No sublimation occurs between 600 and 800 °C, while for a 900 °C process a discrepancy is observed. (b) SEM micrograph of a section of a sample after an 800 °C thermal process.

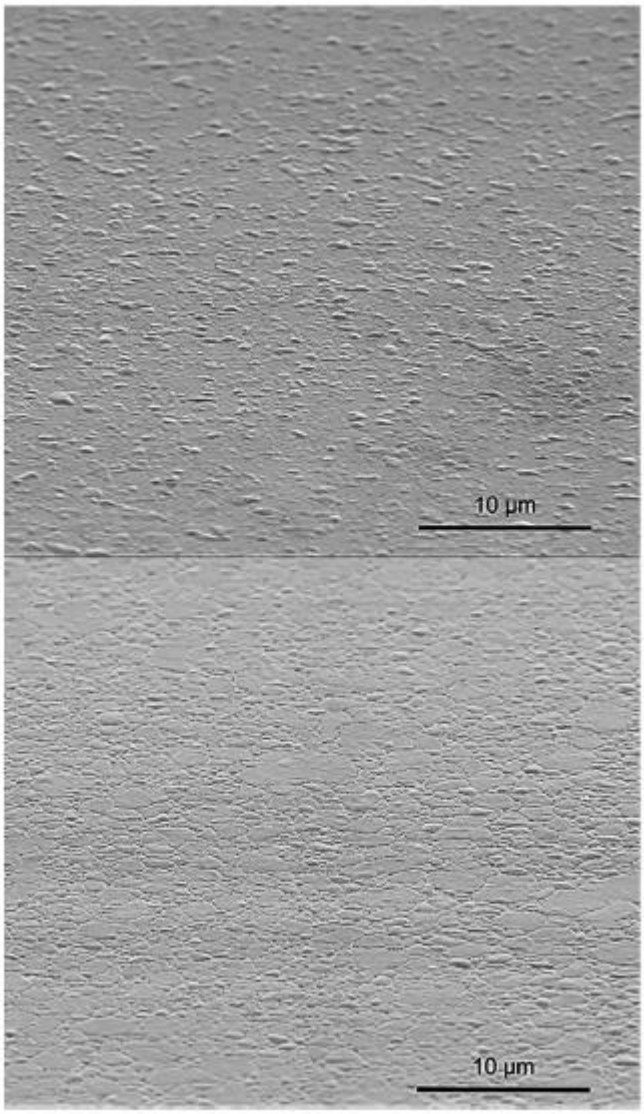

Fig. 6. Tilted SEM images of Cu films, 200 nm thick, heated up to 700 °C in vacuum (top) and H_2 atmosphere (bottom), promptly cooled and extracted out of the chamber. The percentage of bumped grains is reduced in the presence of H_2.

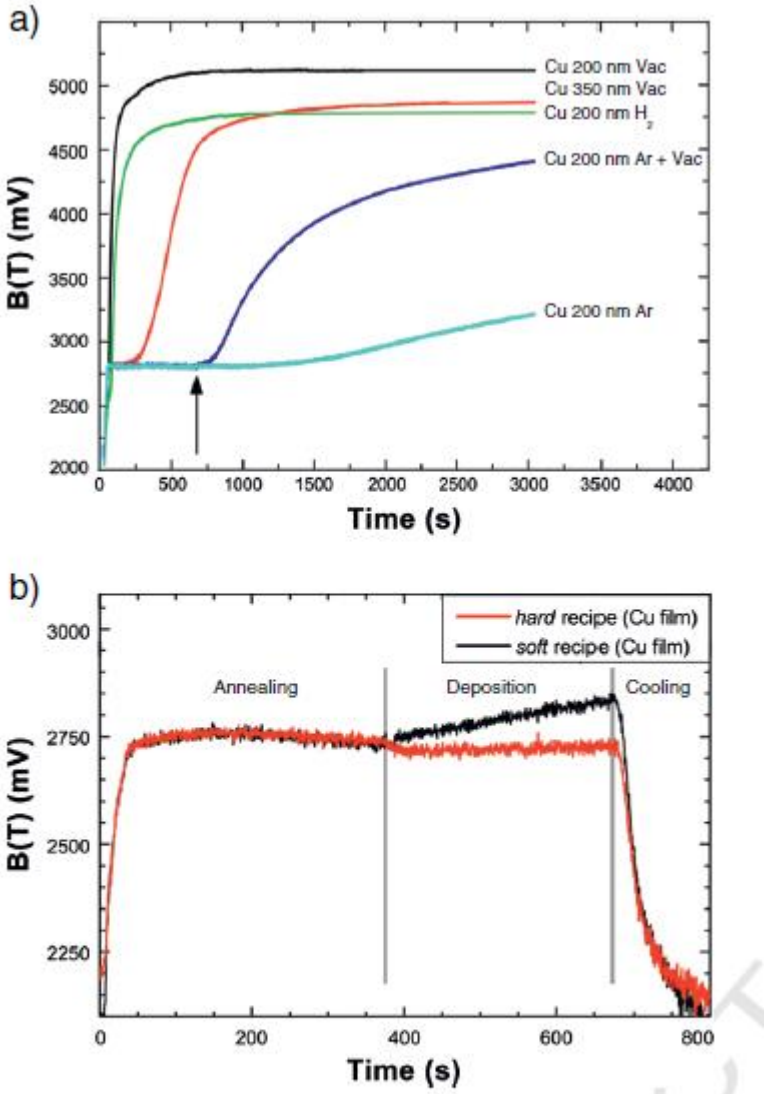

Fig. 7. (a) A collection of dewetting curves obtained at different conditions and T = 800 °C. The arrow indicates the interruption of Ar flux in the chamber in the Ar + vacuum process. In the case of gas flow (green and cyan curves), the pressure was kept at 25 Pa. (b) Evolution of the pyrometer signals during the *hard* and *soft* recipes (T = 700 °C). (For interpretation of the references to color in this figure legend, the reader is referred to the web version of this article.)

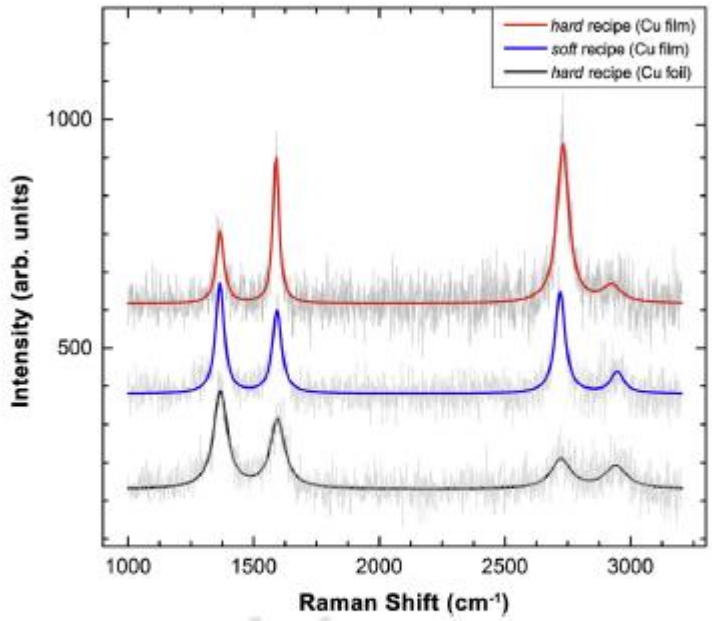

Fig. 8. Typical Raman spectra of graphene deposited on Cu by means of the processes described in the text at T = 700 °C. From top to bottom: *hard* recipe (red), *soft* recipe (blue), and foil (with *hard* recipe in this case, but results do not depend on the pre-treatment). To avoid background luminescence from Cu, illumination at 442 nm has been employed [14]. (For interpretation of the references to color in this figure legend, the reader is referred to the web version of this article.)